Wind-tunnel experiments and separation control of a NACA4412 with 25° sweep at high Reynolds numbers

Pierre-Yves Passaggia, Guillermo Lopez Quesada, Stéphane Loyer, Azeddine Kourta, Lucien Baldas, Stéphane Orieux, Ahmad Batikh, Jean-Christophe Robinet, Bruno Stefes, Nicolas Mazellier

Wind-tunnel experiments and separation control of a NACA 4412 with 25° sweep at high Reynolds numbers

Pierre-Yves Passaggia*
University of Orléans, INSA-CVL, PRISME, EA 4229, 45072 Orléans, France

Guillermo Lopez Quesada†
Institut Clément Ader (ICA), Université de Toulouse, CNRS, INSA, ISAE-SUPAERO, Mines-Albi, UPS, Toulouse, France

Stéphane Loyer‡
University of Orléans, INSA-CVL, PRISME, EA 4229, 45072 Orléans, France

Azeddine Kourta§
University of Orléans, INSA-CVL, PRISME, EA 4229, 45072 Orléans, France

Lucien Baldas, Stéphane Orieux and Ahmad Batikh¶
Institut Clément Ader (ICA), Université de Toulouse, CNRS, INSA, ISAE-SUPAERO, Mines-Albi, UPS, Toulouse, France

Jean-Christophe Robinet‖
Laboratoire DynFluid, Arts et Métiers ParisTech, 75013 Paris Cedex, France

Bruno Stefes**
Airbus Operations GmbH, Bremen, Germany

Nicolas Mazellier††
University of Orléans, INSA-CVL, PRISME, EA 4229, 45072 Orléans, France

Boundary-layer separation at large Reynolds numbers over swept wings remains a challenging phenomenon to either replicate in well-controlled laboratory experiments or predict in full-scale applications. The present work reports the aerodynamic performances of a wind tunnel model based on a NACA 4412 airfoil with a sweep angle of 25° at Reynolds number up to 10^6. Numerical simulations are performed alongside experiments together with a sensitivity analysis which provides important guidelines for the location and injection angle of net-mass-flow actuators such as pulsed jet actuators which allow for controlling the velocity and the frequency of the flow-control strategy independently. In addition, a novel flow-control strategy based on bi-stable fluidic oscillators is presented where the pulsed jet actuators are capable of reaching frequencies of several kHz and Mach numbers close to 0.5. The final setup will consider the control of flow separation at high angles of attack with the objective to improve the aerodynamic performances of the wing.

I. Nomenclature

β = sweep angle
ν = air kinematic viscosity

*Professor, Laboratoire PRISME, pierre-yves.passaggia@univ-orleans.fr
†Postdoc, Institut Clément Ader, glopezqu@insa-toulouse.fr
‡Engineer, Laboratoire PRISME, stephane.loyer@univ-orleans.fr
§Professor, Laboratoire PRISME, azeddine.kourta@univ-orleans.fr
¶Professor, Institut Clément Ader, baldas@insa-toulouse.fr
‖Professor, Laboratoire DynFluid, jean-christophe.robinet@ensam.eu
**Dr.-Ing., Airbus Operations GmbH, bruno.stefes@airbus.com
††Professor, Laboratoire PRISME, nicolas.mazellier@univ-orleans.fr

ρ = air density
θ = angle
AR = wing aspect ratio
AoA = angle of attack
C_p = pressure coefficient
C_D = drag coefficient
C_L = lift coefficient
c = chord
c_0 = speed of sound
D = drag force
L = lift force
M = Mach number
p = local static pressure
p_∞ = free-stream static pressure
Re_c = Reynolds number based on the chord
S = wing surface area
T_∞ = free-stream temperature
u = horizontal velocity
v = vertical velocity
U_∞ = free-stream velocity
w = wing span
f = oscillatory frequency
c_0 = velocity of the pressure wave
L_f = feedback loop length

II. Introduction

TAKE-off and landing are critical flight phases where the pitch of the airplane and the angle of attack AoA with respect to the air flow may lead to detrimental effects such as the onset of stall resulting in loss of lift and drag increase, which ultimately leads to an increase in fuel consumption and/or safety issues. Although the stalling process is now well understood and documented, the physics of turbulent boundary separation [1], and in particular its control using active methods [2], is still a very active area of research [3]. While progress in flow control on laboratory experiments shows promising potential [4], the extrapolation to full scale aircraft remains a challenge posed by the overall efficiency of the embedded system into the aircraft. So far, embedding active flow control devices leading to a net gain in the energy balance on a full-scale aircraft remains an open issue which we attempt to address in the H2020 CleanSky PERSEUS project. To this end, two main objectives are targeted: (i) the design of a new generation of Pulsed-Jet Actuators (PJAs) capable to be operated over a wide range of frequencies at low flow rate penalty and (ii) the development of a new methodology to optimise the PJA internal design (size, aspect ratio) as well as their operating parameters (location/position at the wing, jet blowing amplitude and frequency). Here, the focus is put on the former objective. In this study, active flow control (AFC) is performed using a bi-stable fluidic oscillator [5]. The AFC effectiveness is assessed via the aerodynamic performances of a NACA 4412 airfoil with a sweep angle $\beta = 25°$ over a wide range of operating conditions. Numerical simulations together with a sensitivity analysis are also used in order to determine the most sensible location and injection angle to an AFC device such as PJAs.

This paper is organised as follows. Firstly, the experimental facility used to carry out the aerodynamic study is presented. Aerodynamic performances of the airfoil without flow control are then reported. Secondly, numerical simulations of the same flow configuration than in the wind tunnel is performed for validation while a sensitivity analysis is used to determine the most sensible region of the flow as well as its characteristics to an AFC strategy. Thirdly, the main features of the active flow-control device are detailed. Finally, we emphasise further insights on the coupling of the airfoil model with the AFC will be presented during the conference, and in particular, the flow physics associated with the control that will be investigated in the very near future.

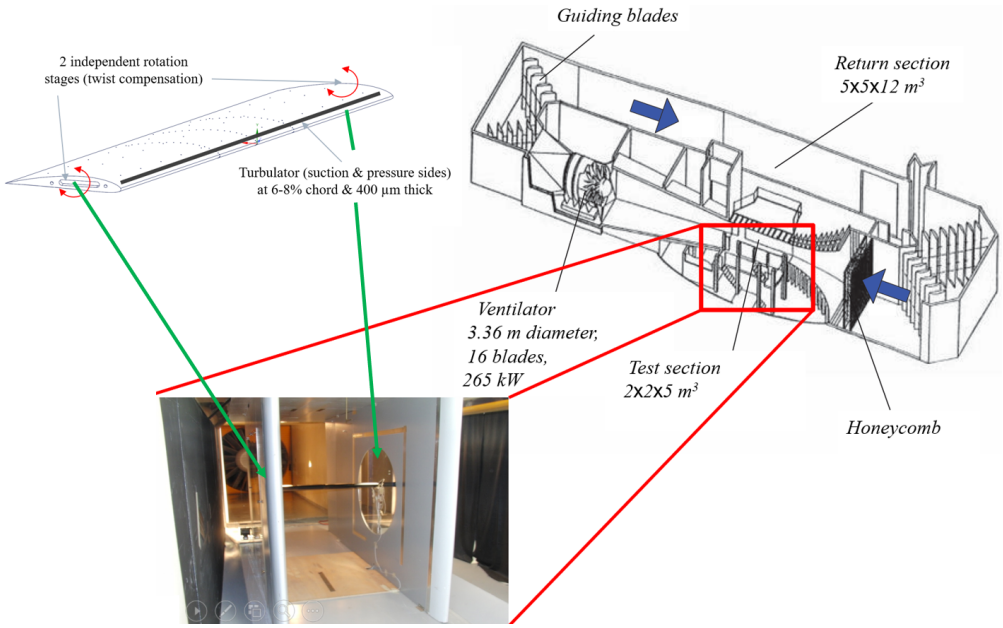

Fig. 1 Sketch of the wind tunnel, the test section, and the model.

III. Wind-tunnel tests

A. Experimental set-up

Experiments were carried out in the S1 wind tunnel at PRISME laboratory (Orléans, France). The test section of this closed-loop wind tunnel is a 2×2 m^2 square, extending over 5 m. The airfoil model is an epoxy made NACA 4412 with a sweep angle $\beta = 25°$ and a constant chord $c = 300$ mm along the wingspan. In this study, the wind speed U_∞ ranges from 10 m/s to 50 m/s, which leads to chord-based Reynolds number $Re_c = U_\infty c/\nu$ (with ν the kinematic viscosity of air) up to 10^6. To mitigate the interference with the boundary layers developing along the wind-tunnel walls, the airfoil model has been set between two side walls installed within the test section as illustrated in Fig. 1. The distance between the side walls is 1100 mm leading to an airfoil aspect ratio of $AR \approx 3.7$. Furthermore, laminar-to-turbulent boundary layer transition on the airfoil is triggered by means or zig-zag turbulators (0.4 mm thick) located at 7% of the chord from the leading edge on both suction and pressure sides. The airfoil is clamped on two discs equipped with two independent rotation stages enabling the variation of the angle of attack AoA over the range $[-10°, 20°]$ and compensating for hysteresis due to model twist. The investigated free-stream velocity, monitored by a Pitot probe located at 1 m from the beginning of the straighteners, is $U_\infty \pm 1.5\%$ m/s. The static pressure tap of the Pitot tube is used as a reference pressure p_∞. The aerodynamic loads experienced by the model are measured by means of a 6-component balance. In addition, 156 pressure taps are used to investigate the pressure distribution around the airfoil.

B. Wind-tunnel results without AFC

The lift coefficient $C_L = 2L/\rho S U_\infty^2$ and the drag coefficient $C_D = 2D/\rho S U_\infty^2$ are computed using both the force balance and the integration of the pressure coefficient $C_p \equiv 2(p - p_\infty)/\rho U_\infty^2$ along the chord at midspan (see Figs. 2(a) and 2(b)). Here ρ is the density of the fluid, S is the surface area of the wing while L and D are the lift and drag forces measured by the force balance. Our results are compared to those from [7] who performed measurements on a unswept NACA 4412 (i.e. $\beta = 0$) and the recent Large Eddy Simulation (LES) reported in [6] for the same flow geometry and at an angle of attack $AoA = 5°$. Note that both measurements from [7] and [6] were corrected with the sweep angle (i.e. multiplied by $\cos(\beta)$). Lift coefficients values are in good agreement as far as 3D effects induced by the swept geometry remain marginal. The departure observed for AoA beyond 10° coincides with the cross-stream flow evidenced by tuft visualisations reported in Fig. 3(a). Note that the LES predicts a lift coefficient slightly higher than that observed experimentally, which may be due to finite size effect in experiments. The drag coefficient is shown in Fig. 2(b) where all values collapse, except for a small shift observed from our force balance. This extra drag is caused in large parts

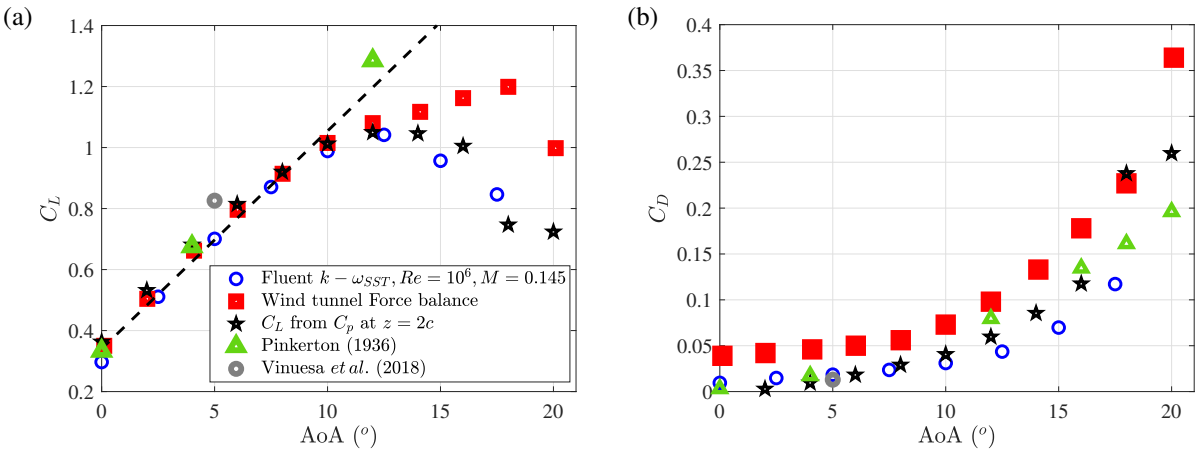

Fig. 2 Comparison for (a) the lift coefficient and (b) the drag coefficient between the force balance (red squares) and the integration of the pressure coefficient (black pentagrams) computed at the mid span. The grey dot reports the values from the high-fidelity numerical simulation [6] and the green triangles correspond to the experiment from [7]. The blue dots report the results from the numerical simulations presented in the next subsection. Note that both results from [6, 7] where corrected using the sweep angle for consistency.

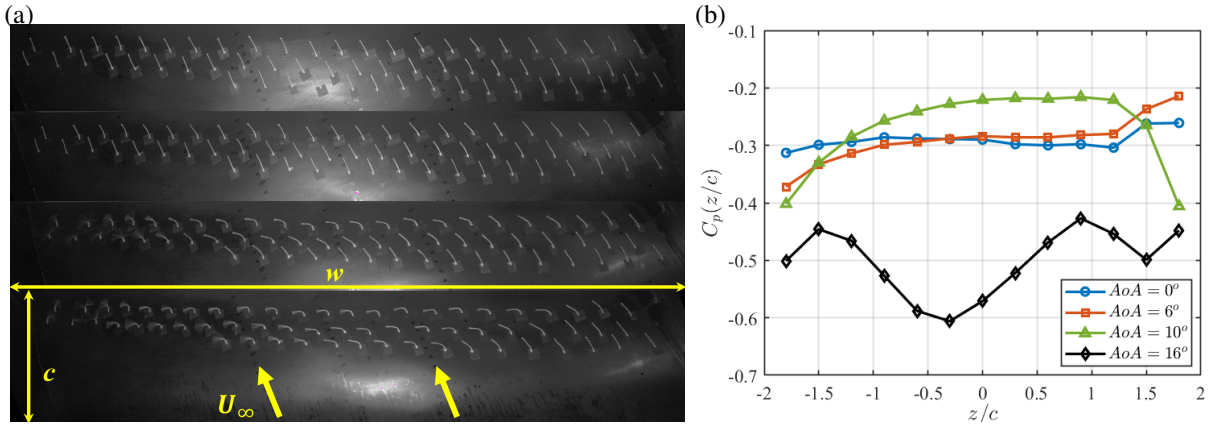

Fig. 3 (a) Tuft visualisation for $AoA = [0, 6, 10, 16]^\circ$ increasing from top to bottom view. (b) Pressure coefficient distribution along the span at $x/c = 70\%$. Both figures are shown for $AoA = [0, 6, 10, 16]^\circ$ and $Re_c \approx 10^6$.

by the friction induced by the supporting discs which are nearly four times the surface area of the wing. The drag coefficient increases rapidly for $AoA > 10^\circ$ but this increase is continuous which confirms that the separation point moves progressively towards the leading edge as AoA increases. For $AoA < 15^\circ$, the lift coefficient calculated from the force balance is in close agreement with that inferred from pressure distribution. For $AoA > 15^\circ$, the measurements from the force balance begin to depart from the lift predicted by the integration of the pressure coefficient. The split between both methods remains somewhat consistent for $AoA > 12^\circ$ although the pressure coefficient is only integrated at mid span. The inflection of the drag coefficient shown in Fig. 2(a) corresponds to the transition from trailing-edge to leading edge separation where the separation along the suction side has to become spanwise dependent. At this point, separation occurs earlier than for the case of the unswept airfoil model which triggers separation for a larger AoA.

To investigate further the influence of the swept geometry, tuft visualisations are compared to spanwise pressure distribution in Fig. 3 with respect to AoA. Tuft visualisations are reported in Fig. 3(a) for four AoA showing the sequence leading to static stall. For increasing angles of attack, the flow on the suction side progressively aligns and sweeps along the span of the wing. Note that for $AoA = 16^\circ$, tuft visualisations show that the separation point becomes progressively non uniform and that separation becomes span dependent. This observation is further confirmed in Fig. 3(b) where the spanwise distribution of the pressure coefficient at $z/c = 70\%$. For $AoA \leq 10^o$, the pressure in the

span is essentially constant. The pressure gradient is therefore very small and independent of the spanwise position. Nonetheless, near the supporting discs, a residual pressure gradient is observed and is either favourable or adverse for the left and right ends, respectively. At the contrary, for $AoA > 16^o$, the spanwise evolution of the pressure coefficient becomes irregular and the separation region may no longer be expected to be two-dimensional. At this point, it is unclear whether this spanwise pressure gradient is caused by a stall cell, finite-span effects, or a combination of both.

C. Numerical validation and sensitivity analysis

In addition to previous experiments on the same flow geometry, numerical simulations were carried out using ANSYS Fluent 2021 R2 to further validate the present experiment using a Reynolds-Averaged-Navier-Stokes commercial solver, and the adjoint solver provided in the package was used in order to provide guidelines for the design of the pulsed-jet actuators such as optimal chord-wise location and optimal jet angle.

Numerical simulations were carried out on a three-dimensional C-type grid as shown in figure 4(a) where the mesh comprises 478,000 elements organised in a structured-type mesh although the mesh is treated as unstructured. The Mach number $M \equiv U_\infty/c_0 = 0.145$ was set as a free-stream condition and the Reynolds number was set to $Re = 10^6$, similarly to the experiment. Here c_0 is the speed of sound. The computational domain extends 10 chords upstream, below and above the airfoil, while the computational domain extends 20 chords downstream the airfoil. The sweep angle was also set at $\beta = 25°$ in the simulation, similarly to the experiment. The flow solver is incompressible and uses a second-order upwind type scheme for the advection terms and a SIMPLEC projection scheme for the pressure. A $k-\omega$ turbulence model based on the shear-stress transport equation developed in [8] was employed for turbulence modelling while a value of $y^+ < 1$ was ensured for both the suction and the pressure sides of the airfoil. The width of the domain was kept intentionally small with a span equal to 1% of the chord. Results are compared side-by-side with the experiment in Fig. (2)(a) for the lift coefficient C_L and in Fig. (2)(a) for the drag coefficient C_D. The comparison is accurate for the C_L until $AoA > 14°$ when compared with the integrated pressure coefficient at the mid span. The comparison with the drag coefficient is also very good and follows the same prediction than the experiment and previous investigations on the same wing profile from the literature.

The mean horizontal velocity computed at $AoA = 14^o$ is shown in 4(b) where the onset of incipient separation can be observed at $x/c \approx 0.5$. The distribution of the pressure coefficient along the chord $C_p(x/c)$, computed at $AoA = 10°$ is shown in Fig. 4(c) and shows very good agreement, at least for this pre-stall angle of attack. The onset stall was found at $AoA \approx 14°$ and the pressure coefficient on the airfoil still shows very good agreement with the experiment as shown in Fig. 4(d). A sensitivity analysis was then conducted using this steady state obtained at $AoA = 14°$ as a baseflow to compute the sensitivity of the lift-to-drag ratio (i.e. C_L/C_D) to a steady momentum body force in the flow and at the boundary of the wing. The sensitivity of the lift-to-drag ratio to a momentum body force in the horizontal and vertical directions is shown in Fig. 4(e). The most sensitive region to the actuation of the flow is found to be located in a wide region $0.05 < x/c < 0.5$ and nearly half the suction side. It is however interesting to note that the sensitivity is not peaked at a particular location and that it decreases when approaching the separation region $x/c \approx 0.5$. In other words, the actuator should remain efficient for most locations located upstream the separation region. The relative angle between the optimal actuation and wing is shown in Fig. 4(f) where the angle remains essentially constant for $0 < x/c < 0.2$ with a value around 14° relative to the tangent to the wing. This angle confirms that a Coanda-type effect in the boundary layer seems to be the most sensitive way to improve the lift-to-drag ratio and thereby control separation.

Next we present a PJA device based on fluidic oscillators that aims at suppressing separation for the stall conditions for the present aerodynamic control parameters.

IV. Design and integration of novel Pulsed Jet Actuators

The PJAs introduced in this work are based on fluidic oscillators [5] with some modifications in order to make them suitable for integration in the NACA4412 airfoil. These new PJAs (Fig. 5(a)) consist of one inlet nozzle connected to a switching zone that is divided in two long channels (S1 and S2) by a splitter, each of them leading towards a feedback loop (F1 and F2). These feedback loops reconnect to the switching zone through their respective control ports (C1 and C2). At the beginning of each feedback loop an elbow connects with a reservoir and the outlet channels (O1 and O2).

The oscillatory behaviour of the actuator is provided by the feedback-loop geometry and the control ports connected to the switching zone. Considering for example an initial flow from the inlet nozzle attached, thanks to the Coanda effect, to the splitter channel S1 (blue flow in Fig. 5), part of the flow would exit from the actuator through the outlet O1 while

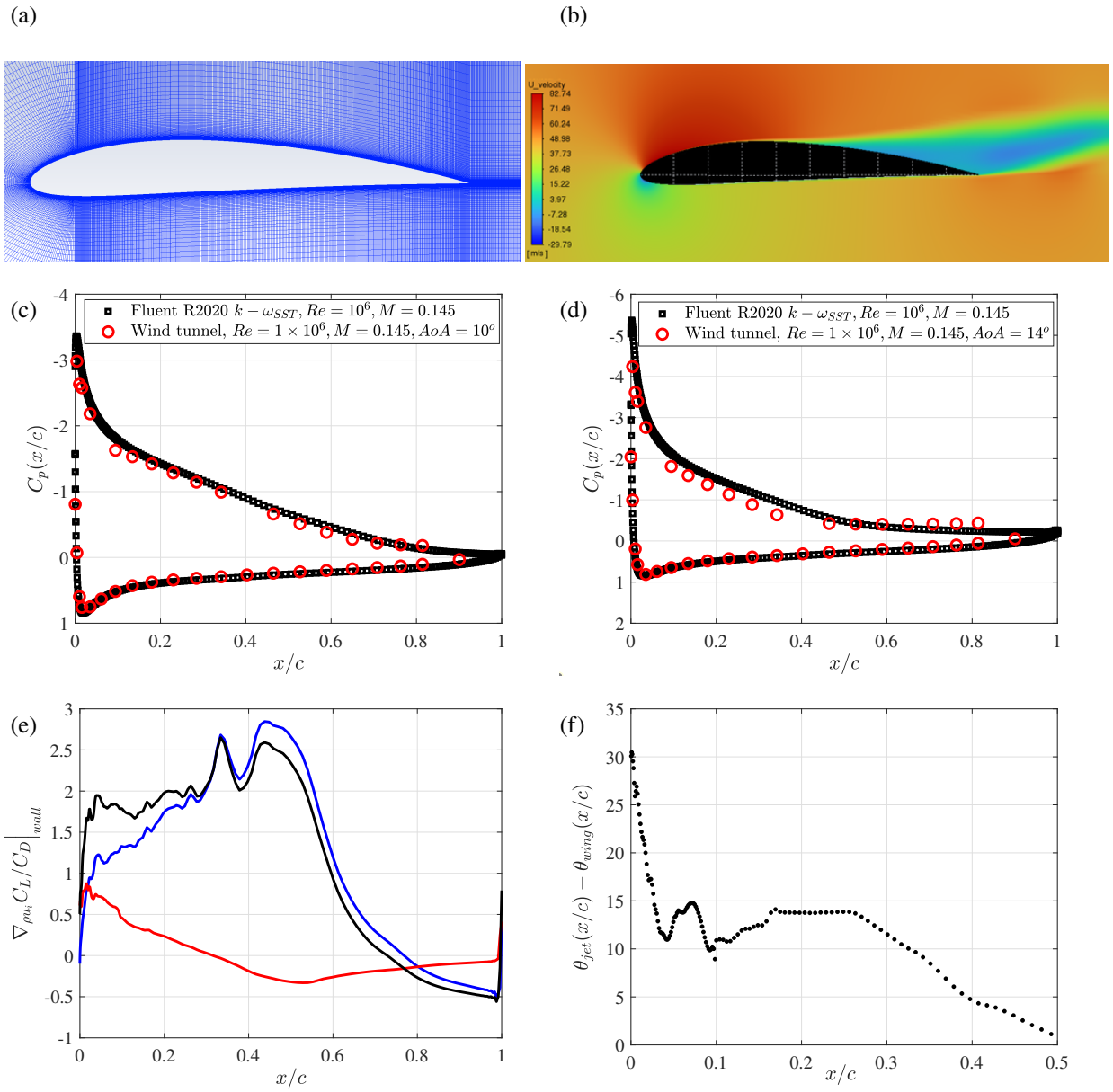

Fig. 4 (a) Close up view of the mesh, (b) mean horizontal velocity ($U(x,y)$) for $AoA = 14^o$, (c) pressure coefficient distribution $C_p(x/c)$ computed at $AoA = 10^o$ for the experiment (○) and the simulation (●). (d) Same as (c) but for $AoA = 14^o$. (e) Sensitivity of the mean flow to a body force acting on the horizontal momentum ρu (blue), the vertical momentum component ρv (red), and sum of both components (black) computed along the suction side. (f) Relative angle (^{o}) between the sensitivity shown in (e) and the local angle along the suction side of the airfoil.

the rest of the flow would run along the feedback loop F1 and its corresponding control port C1, increasing the pressure in this loop with a compression wave propagating roughly at the speed of sound. When this pressure wave reaches C1, it is reflected back and provokes a pressure increase at the connection between F1 and S1. The same phenomena occur but with expansion waves on the other side of the oscillator. Thus, the pressure imbalance between S1 and S2 together with pressure imbalance between C1 (control port with flow, higher pressure) and C2 (control port without flow, lower pressure), results in the switching of the flow stream from S1 (blue flow) towards S2 (red flow). Then this process is repeated in the same way for the opposite feedback loop F2 and control port C2, providing the oscillatory change of the flow stream from S1 to S2 and effectively generating pulsating jets at the outlets O1 and O2. Therefore, the main

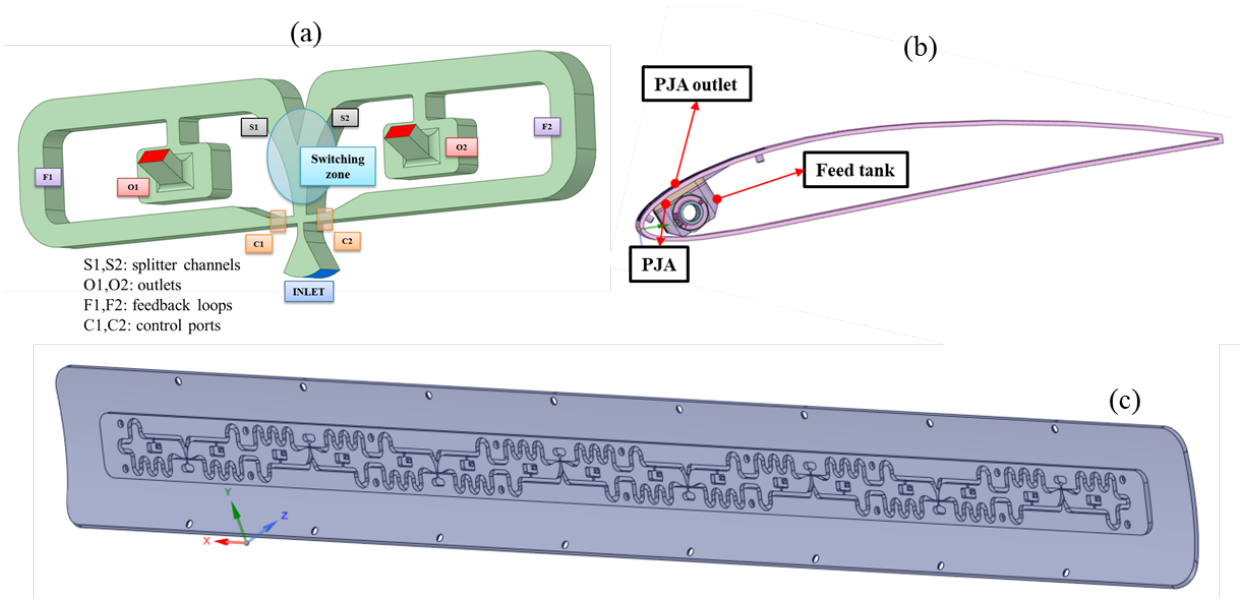

Fig. 5 (a) Geometry of a single PJA, (b) integration of the PJA in the airfoil and (c) PJA assembly showing the interconnected synchronised oscillators.

control parameter for the frequency f of oscillation is typically the length L of the feedback loop through the following expression $f = c_0/4L_f$ [5]. Since the objective is to allow flow control along the span of the wing, a large assembly of oscillators is required. If the oscillators were left independent from each other, their oscillatory frequencies could vary or have different phases due to manufacturing imperfections or variations in the operating conditions. However, the proposed design allows for a natural synchronisation of the assembly by connecting the feedback loops of any oscillator with the control port of the adjacent ones (Fig. 5(c)).

As demonstrated in the previous section, the most sensitive region to the actuation of the flow is located on the first half of the suction side. The typical dimensions of the experimental airfoil result on a very limited space for the implementation of the PJAs inside the airfoil (Fig. 5(b)). The PJA assembly will be design accordingly in three different positions for the actuation that are proposed to be evaluated in the chord like direction (5%, 10%, and 15% of the chord length).

To obtain suitable frequencies (below 800 Hz) for the separation control theoretically requires feedback loop lengths longer than 100 mm. Since the space allocated for the feedback loops is very limited due to the geometrical constraints, modifications on the internal design of previous fluidic oscillators found in the literature are required. The numerical investigation has been then focused on reducing the frequency for shorter feedback loops by modifying the splitter area of the oscillator as well as increasing the complexity of the feedback loop while keeping a proper switching of the jet. The numerical investigation has been performed with ANSYS Fluent using a coupled solver, second-order discretization scheme and the realizable $k-\epsilon$ turbulent model. Several 3D models of at least 2 synchronised oscillators (2 inlets, 4 outlets) have been simulated with a time-step size of the unsteady simulation of 10^{-5} s and an unstructured mesh of at least 7 million cells. The numerical study has been focused on characterising the outlet jet velocities and the frequency of oscillation (Fig. 6(a)).

The numerical investigation shows that round external walls at the splitter help stabilising the switching of the jet, while generating recirculation zones and increasing the complexity of the feedback loops decrease the frequency of oscillation compared to previous works. In Fig. 6(b) the average velocity at the outlets of a traditional design with straight splitter walls and simple feedback loops (top) is compared to an improved design with round external splitter walls, recirculation zones and more complex feedback loops (bottom). The frequency of oscillation is almost half in the improved design even though the length of the feedback loop in the traditional design is 30% longer than the improved design. Additionally, although the velocity profile in the classical design is smoother, the amplitude of the oscillation is larger in the improved design, which may also be beneficial for the actuation performance of the PJAs to control separation over the airfoil.

The resulting designs selected from the numerical investigation are being manufactured by 3D printing to perfectly

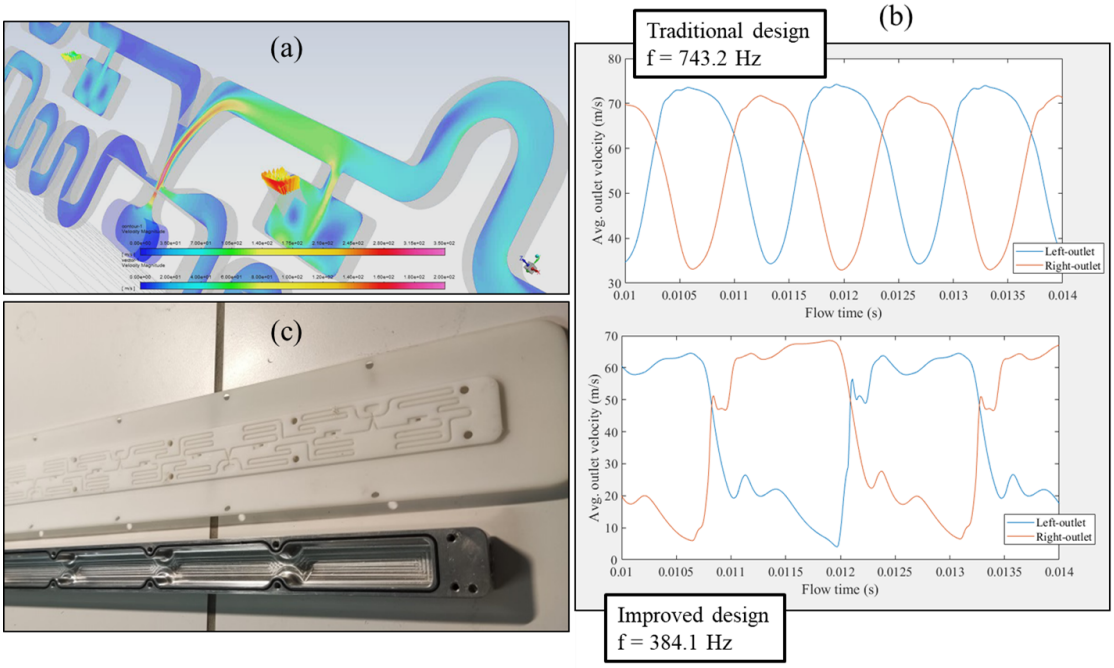

Fig. 6 (a) Velocity field in the mid plane and velocity vectors at the outlet of a PJA assembly, (b) average velocity profile at the outlets of traditional (top) and improved PJA (bottom) designs with feedback loop length of 190 mm and 137 mm respectively and (c) 3D printed sample of a PJA assembly.

adjust to the curvature of the NACA 4412 airfoil. Additionally, with the 3D printing process, it is possible to manufacture the outlets so that the pulsed jets flow in a nearly tangential direction with respect to the airfoil surface (as hinted by the sensitivity analysis) to improve the efficiency of the actuation for delaying the flow separation. As shown in (Fig. 6(c)), the 3D printed PJA assembly consist of two parts: one corresponding to the 3D printed cover containing the actuators while the other one is a long aluminium reservoir to provide the gas feed for each oscillator. In the interface between them an aluminium plate covers the whole PJA assembly only allowing the pressurised air from the feed tank to flow through the inlet nozzle.

Initially, three different PJA assemblies corresponding to the previously introduced aspect-ratio and spacing are being manufactured to be tested in the 10% chord length position. For the 5% and 15% chord length position, new PJA assemblies shall be manufactured since the curvature of the NACA 4412 airfoil is not constant. In the end, a total of nine PJA assemblies are to be manufactured and integrated within the NACA 4412 airfoil for wind tunnel experiments. The full characterisation of these PJA assemblies will be provided before their implementation in the NACA 4412 airfoil for wind-tunnel testing.

V. Conclusions and Outlook

A series of experiments has been performed on a swept NACA 4412 airfoil varying angle of attack and Reynolds number. The lift and drag coefficients compare faithfully with previously reported results as far as swept-induced 3D effects stays marginal. Reynolds-averaged numerical simulations were performed alongside and confirmed the possibility to predict the aerodynamic performances for the same flow conditions than in the experiment. In addition, a sensitivity analysis demonstrates that in order to improve the aerodynamic performances (i.e. the lift-to-drag ratio), actuators should be located upstream the separation region without a particular emphasis on the location. However, the sensitivity analysis hints to the importance of injecting momentum tangentially to the boundary layer, with an angle of approximately 14° with respect to the airfoil. Besides, a novel bi-stable fluidic oscillator has been designed with the objective to mitigate the flow separation on the airfoil at high angles of attack. A numerical investigation has been performed in order to adapt the typical designs found in the literature to the constraints given by the implementation of the PJAs (i.e. miniaturization of the device). The results show that modifying the internal flow structure of the oscillator by generating recirculation zones, increasing the complexity of the feedback loops or enforcing the Coanda effect with

round walls in the switching zone, allow for a further tuning of the oscillatory frequency not only dependant on the feedback loop length. It is worth noticing that a wing model equipped with interchangeable arrays of fluidic oscillators is currently manufactured. The next step is therefore to investigate the effect of AFC on aerodynamic performances of the airfoil taking as a reference, the results reported in this abstract. During the conference, a complete set of results will be presented to assess the performances of the control device. A wide range of control parameters, encompassing actuation frequency, actuator spacing and actuator aspect ratio, will be presented.

Acknowledgements

This project has received funding from the Clean Sky 2 Joint Undertaking (JU) under grant agreement No 887010. The JU receives support from the European Union's Horizon 2020 research and innovation programme and the Clean Sky 2 JU members other than the Union. The financial support of the Region Centre Val de Loire, EFRD, European Funds for Regional Development, and CPER (project PROMESTOCK) is also acknowledged.

References

[1] Simpson, R. L., "Turbulent boundary-layer separation," *Ann. Rev. Fluid Mech.*, Vol. 21, No. 1, 1989, pp. 205–232.

[2] Lachmann, G. V., *Boundary layer and flow control: its principles and application*, Elsevier, 2014.

[3] Cattafesta III, L. N., and Sheplak, M., "Actuators for active flow control," *Ann. Rev. Fluid Mech.*, Vol. 43, 2011, pp. 247–272.

[4] Seifert, A., Darabi, A., and Wyganski, I., "Delay of airfoil stall by periodic excitation," *J. Airc.*, Vol. 33, No. 4, 1996, pp. 691–698.

[5] Wang, S., Batikh, A., Baldas, L., Kourta, A., Mazellier, N., Colin, S., and Orieux, S., "On the modelling of the switching mechanisms of a Coanda fluidic oscillator," *Sensors and Actuators A: Physical* , Vol. 299, 2019, p. 111618. https://doi.org/10.1016/j.sna.2019.111618, URL https://hal.archives-ouvertes.fr/hal-02297254.

[6] Vinuesa, R., Negi, P. S., Atzori, M., Hanifi, A., Henningson, D. S., and Schlatter, P., "Turbulent boundary layers around wing sections up to Rec= 1,000,000," *Int. J. Heat & Fluid Flow*, Vol. 72, 2018, pp. 86–99.

[7] Pinkerton, R. M., *Calculated and measured pressure distributions over the midspan section of the NACA 4412 airfoil*, Vol. 563, NACA T. R., 1936.

[8] Menter, F. R., "Two-equation eddy-viscosity turbulence models for engineering applications," *AIAA J.*, Vol. 32, No. 8, 1994, pp. 1598–1605.